Dynamic Observation of Magnetic Particles in Continuous Flow Devices by Tunneling Magnetoresistance Sensors

A. Weddemann,* A. Auge, F. Wittbracht, C. Albon, and A. Hütten
Department of Physics, Thin Films and Physics of Nanostructures, Bielefeld University
*Universitätsstr. 25, 33615 Bielefeld, Germany, *weddeman@physik.uni-bielefeld.de*

Abstract: Dynamic measurement of magnetic particles in continuous flow devices is made very difficult by the limitations imposed by the sensors themselves. Thus, certain sensor layouts are restricted to either number sensitive or spatial resolutive measurements of magnetic particles. We investigate different new strategies to increase the detection threshold and introduce designs accomplishing both: detection giving information about number and positions of particles. For this purpose we introduce sensors of non-linear magnetization behaviour by varying the sensor geometry.

Keywords: ferromagnetism, micromagnetism, magnetic particles, magnetoresistive sensors

1. Introduction

The observation and detection of objects in continuous flow devices is often helpful to understand the ongoing dynamics. Especially, in many lab-on-a-chip applications a direct optical analysis is not possible e.g. since the size of biological molecules lies below the resolution limit of such microscopes. A possible strategy to make them visible is to combine them with a magnetic marker for example a magnetic bead on the nano- or microscale. Those can be detected by magnetoresistive sensors due to their stray field and therefore enable an indirect detection of the biomolecule itself. It was proven that a magnetic detection of static and moving particles is possible.[1,2] However, to obtain a proper sensor signal, the resistance change needs to be above a certain noise threshold. Due to a rapidly decreasing stray field, this imposes strong restrictions on the distance between particles and sensor. Commonly, difficulties are already encountered, if the distance is above three times the particle radius. Therefore, it is an important task to adjust the sensors to the particles to be detected. Here we will study different influences on the sensor signal obtaining guidelines on how to design future sensor layouts.

2. Governing equations

Magnetoresistive sensors usually consist of a huge amount of components of different materials. However, the simplest system is given by two ferromagnetic layers that are separated by a non-magnetic either conductive or insulating barrier. The total resistance of such systems depends on the relative orientation of the magnetization $\boldsymbol{M}$ in each layer. A magnetic particle close to the sensor influences this magnetic configuration and thus leads to a resistance change ΔR. The norm of the magnetization $\boldsymbol{M}$ is a material constant, the saturation magnetization M_S. Therefore, the information of the layer is given by the orientation of the direction vector $\hat{\boldsymbol{m}} = \boldsymbol{M} / M_S$ at every space point. Its equilibrium state can be derived from the equation for static micromagnetism

$$\hat{\boldsymbol{m}} \times \boldsymbol{H}_{\text{eff}} = \boldsymbol{0} \tag{1}$$

with the effective magnetic field

$$\boldsymbol{H}_{\text{eff}} = \frac{2A}{\mu_0 M_S}(\nabla \hat{\boldsymbol{m}})^2 + \frac{\delta f_{\text{ani}}(\hat{\boldsymbol{m}})}{\delta \hat{\boldsymbol{m}}} + \boldsymbol{H}_{\text{demag}} + \boldsymbol{H}_{\text{ex}} . \tag{2}$$

The first summand in (2) originates from magnetic exchange coupling, it leads to a parallel alignment of “neighboring” magnetic moments. The material parameter A denotes the exchange constant that is a measure of how stiff the magnetic material is in respect to a change of the magnetization orientation in respect to space. The microscopic crystal structure introduces directions within the material that are energetically more favourable than other. The information on the relation between direction and energy is given by the anisotropy functional f_{ani}. The demagnetization field $\boldsymbol{H}_{\text{demag}}$ is generated by the magnetic material $\boldsymbol{M}$ of the ferromagnet. If no external current densities can be found in the system, it can be expressed as gradient of a scalar

potential ϕ, i.e. $\boldsymbol{H} = -\nabla\phi$. The governing equation for ϕ follows directly from Maxwell equations

$$\Delta\phi = \nabla \boldsymbol{M} \,. \tag{3}$$

Any further external field contributions are summarized in $\boldsymbol{H}_{\text{ext}}$. Especially the particle stray fields have to be included here. We assume spherical homogeneously magnetized particles of magnetic moment $\boldsymbol{m}_{\text{part}}$. The corresponding field is given by the dipole expression

$$\boldsymbol{H}_{\text{bead}}(\boldsymbol{r}) = \frac{1}{4\pi} \cdot \frac{3\langle \boldsymbol{m}_{\text{part}}, \hat{\boldsymbol{r}}\rangle \hat{\boldsymbol{r}} - \boldsymbol{m}_{\text{part}}}{r^3} \,. \tag{4}$$

Particles close to the sensor lead to a resistance change ΔR. If we restrict our analysis to insulating or *tunneling barriers*, the resistance change due to a magnetic field is called *tunnel magnetoresistance* effect (TMR). For quantitative analysis the TMR-ratio is given by[3]

$$\text{TMR} = \frac{\Delta R}{R} = \frac{1}{3}\frac{1-\langle\alpha\rangle}{1+\langle\alpha\rangle/3} \,, \tag{5}$$

$$\langle\alpha\rangle = \frac{1}{A_{\text{layer}}} \int_{A_{\text{layer}}} \cos(\sphericalangle(\hat{\boldsymbol{m}}_1, \hat{\boldsymbol{m}}_2))\, d\boldsymbol{r} \,,$$

if $\hat{\boldsymbol{m}}_1, \hat{\boldsymbol{m}}_2$ denote the magnetization direction within the ferromagnetic layers. It may be pointed out that the layers interact with other via their magnetic stray field as well as additional coupling effects. Considering insulating layers the interface between ferromagnet and insulator commonly is not perfectly smooth but of a certain roughness. Since the thickness d of the insulator is very small (d ~ 1 nm) there is a correlation between the roughnesses on each of the interface. In a simple model proposed by Néel[6] one may assume a structural defect given by a sinusoidal shape of period length λ and a height h. The coupling energy is given by

$$J_{\text{Néel}} = M_S^2 \langle \hat{\boldsymbol{m}}_1, \hat{\boldsymbol{m}}_2 \rangle \cdot \frac{\mu_0 \pi h^2}{\sqrt{2}\lambda} \exp\left(-\frac{2\pi\sqrt{2}d}{\lambda}\right) \,. \tag{6}$$

Stray field layer coupling leads to an antiparallel while Néel-coupling favors a parallel alignment.

3. Model system

Equation (1) together with (6) has been solved for a single probe particle creating a magnetic field according to (4). To investigate the influence of the particle in respect to its position, a grid is introduced, discretizing the space above the sensor. The particle is positioned at each grid point consecutively. The strength of the influence can be measured by means of the average angle distortion $\langle\alpha\rangle$ according to (5). However, as we will still see, with increasing distance, the sensor signal decays rapidly due to a stray field decrease ~ $1/r^3$. Especially for detection in continuous flow devices this leads to strong restriction of which particles or magnetic objects can still be detected. To increase the sensitivity of a sensor a lot of different materials have been considered in the last years. Here we want to use a different approach though, an increased detection threshold by an adjusted sensor layout.

Therefore different setups shall be discussed. The investigated sensor systems are schematically shown in Fig. 1: a) elliptical electrodes of semiaxis lengths of 400 and 100 nm. Magnetic layers have thicknesses of 4 the tunneling barrier a thickness of 2 nm. b) A rectangular sensor with side lengths of 400 and 200 nm, each layer has a thickness of 10 nm. c) A star with five peaks, the layer thickness is again 10 nm. All setups consist of two ferromagnetic layers. As magnetic material we assume CoFeB leading to material parameters $A = 2.86 \cdot 10^{-11}$ J/m and $M_S = 1194$ kA/m.[7]

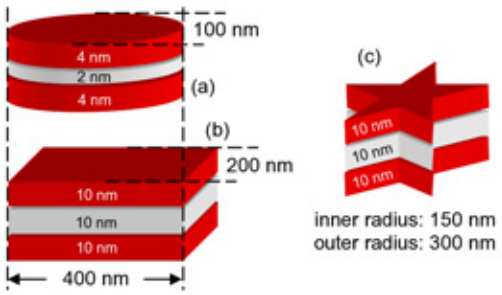

FIG. 1: Different sensor setups. All sensors consist of two magnetic CoFeB-layers that are separated by an insulating tunneling barrier.

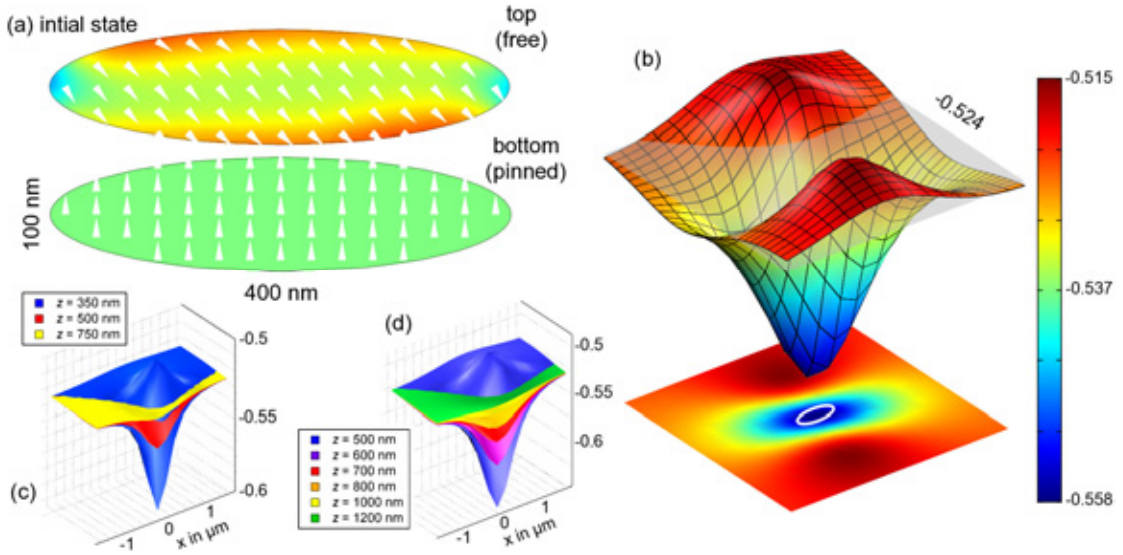

FIG. 2: Elliptical sensor geometries. (a) Due to a bottom layer that is pinned perpendicular to the long semiaxis, the free layer does not align with the easy geometrical axis. (b) shows a $\langle\alpha\rangle$ – surface in respect of the particle position. The mesh indicates the position of the grid nodes, the grey level gives the value without a particle in sensor range. (c) and (d) show the signal decay for different particle distances for particles of a saturation magnetization M_S = 1000 kA/m and radius r = 250 nm (c) and 400 nm (d)

The top electrode will always be free while the bottom one will be chosen free or fixed / *pinned* for several systems. The properties of each sensor design shall now be discussed in detail. As a measure for the particle influence we calculate the average angle distortion according to (5).

3.1 Elliptical geometries

The magnetization in the bottom layer is chosen fixed; its direction is assumed to point parallel to the positive y-axis coinciding with the geometrical hard axis of the ellipse. The alignment of the top layer is governed by an interplay between stray field minimization (alignment parallel to the long semiaxis) and the stray field coupling to the bottom electrode (alignment along the negative y-axis). The resulting state of a system without a particle is shown in Fig. 2(a). The area around the sensor is discretized by the grid nodes

$$x = -1.5\ \mu\text{m} + 0.2\ \mu\text{m} \cdot i \qquad i = 0,...,15$$
$$y = -1.5\ \mu\text{m} + 0.1\ \mu\text{m} \cdot j \qquad j = 0,...,30\,,$$

and different values for the particle height z. Fig. 2(a) shows a typical $\langle\alpha\rangle$ – surface for such a system. For the particle parameters r = 400 nm, M_S = 1000 kA/m and z = 800 nm are chosen; the particle is assumed to be magnetized parallel to the y-axis. By the grey level the value of the free sensor is indicated. A particle on top of the sensor introduces a strong distortion. Depending on the particle position, the sign of the angle change $\langle\alpha\rangle$ may be positive of negative. Such a behvaviour is well suited for applications in spatial detection since the sensor response strongly depends on the particle position.

However, this is bought at some cost. As Fig. 2 (c), (d) indicate the measured signal drops rapidly and commonly quickly falls below the noise signal of such electric devices, the particle can thus not be detected anymore. For the given setup the main reason for this is the stiffness of the free electrode: it is almost homogeneously magnetized and the magnetization direction is strongly influenced by the geometrical anisotropy of the elliptical and the stray field of the bottom electrode. An approach to improve the detection threshold is to introduce very soft magnetic areas along the sensing layer.

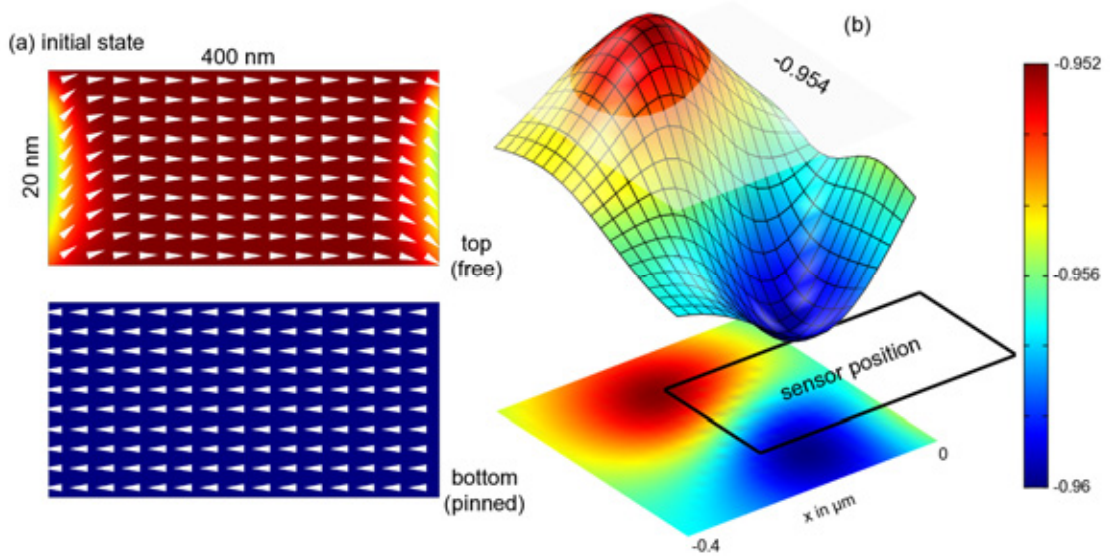

FIG. 3: Rectangular sensor geometries. (a) initial magnetization state under the assumption of a pinned bottom electrode. The sensing free layer reaches a C-state that is align antiparallel to the pinning direction. The short boundary segments show strong curvature which makes them very sensitive. (b) shows the corresponding $\langle\alpha\rangle$ – surface, close to the short rectangle edges strong sensor signal can found even for particle of small momemt (r = 50 nm, M_S = 350 kA/m) and big distance (z = 500 nm).

3.2 Rectangular geometries

A magnetization orientation pointing along the negative x-axis is assumed for bottom pinned layer in this configuration. Due to stray field coupling the top electrode reaches an antiparallel orientation. However, at the boundary segments parallel to the y-axis deviations from a perfectly aligned magnetization distribution can be found (Fig. 2(a)), the electrode shows a C-state. Here the interplay of the demagnetization field of the layer itself (favoring a C- or vortex state), the stray field of the bottom electrode (preferring antiparallel layer alignment) and the exchange energy (minimizing the curvature of the magnetization components) creates a magnetic highly sensitive area. This can easily be influenced by even small magnetic fields. As a probe particle a 100 nm magnetite particle ($M_S \approx$ 350 kA/m) was assumed. Its influence on the sensor for a height of z = 500 nm is shown in Fig. 3. Around the short boundary segments a strong influence can be found. It needs to be pointed out, that a similar effect is not observed at the boundaries parallel to the x-axis. We can therefore conclude that the actual main contribution originates from the equilibrium state of the free layer system and the introduced soft magnetic areas.

Increasing the size of the rectangle would increase the length of the sensitive boundaries. However, it would show that each point along the sensitive areas lead to a similar sensor response while the areas of less sensitivity would not contribute at all. Therefore, such a setup is not a possibility to determine the exact particle position within a flow, it will only respond at the times when a particle passes the sensitive areas. The information that can obtained are thus restricted to “yes/no”-detection (answering the question if there is a particle or not) or a counting device. Another possible application would be velocity measurements: by placing the long edges of the rectangle parallel to the flow direction, both short edges respond at different times for a by traveling particle. The time difference between certain signals can thus be put in relation with the distance the particle passed. Introducing magnetically soft areas proves to be a good strategy for sensor designs. The question arises, how to introduce a high degree of easily switchable areas within the ferromagnetic material. Here we want to focus on geometrical control.

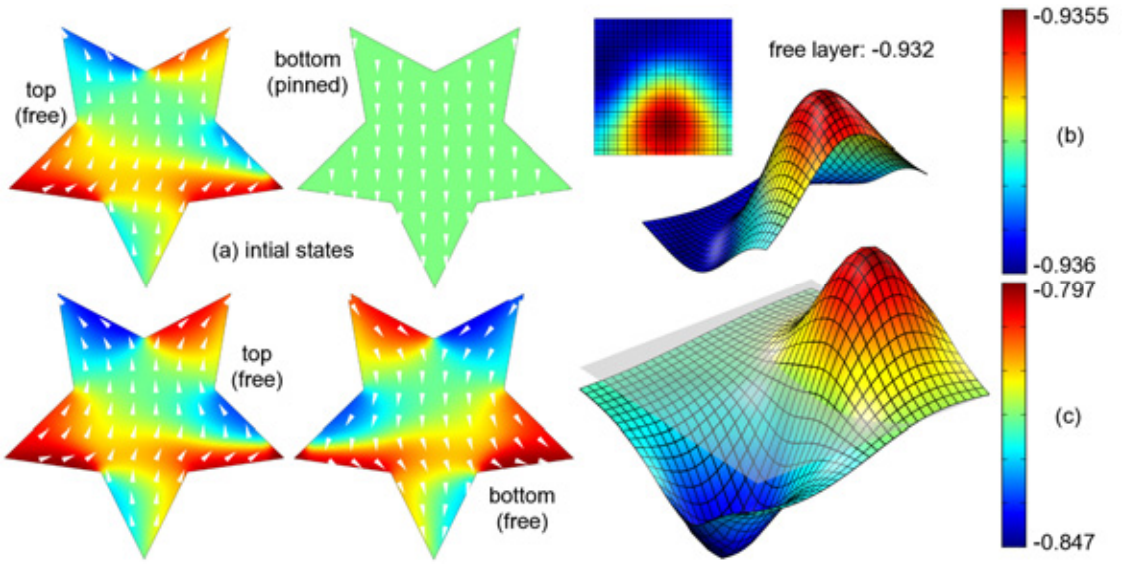

FIG. 4: Star shaped sensor geometries. (a) Different initial conditions are considered: a free sensing top layer with a pinned bottom electrode and two free electrodes. (b), (c) Resulting $\langle\alpha\rangle$ – surface for particles

3.3 Star shaped sensors

In the case of star shaped sensors, two different setups are analyzed: a) sensors with only the top layer free while the bottom electrode is pinned along the positive *y*-axis and b) a system with two free layers. The initial configurations are shown in Fig. 4(a). In the case of only a single free layer (Fig. 4(b)) the highest influence can be found if the particle is placed in the upper half of the sensor (blue area). The peak pointing downwards is again strongly influenced by the magnetic stray field coupling to the bottom ferromagnetic layer. However, upper areas behave less stiffly; particle detection seems to be possible.

To further improve this setup, a free bottom layer is considered. Due to more degrees of freedom, the magnetization process reaches higher complexity; a $\langle\alpha\rangle$ – surface is presented in Fig. 4(c) and shows a totally different behaviour than the preliminary discussed case. The sensitivity is strongly enhanced since both layers can rotate freely. Also, the sign of the measured signal shows a space dependency similar to elliptical sensor elements. Therefore, this combines both advantages of the systems discussed before: it enables space resolute detection at a high sensitivity.

4. Conclusion

In this work, we have proven that the detection threshold of magnetoresistive sensors can be adjusted by a proper sensor shape design. We have shown that introducing magnetically soft areas enables new possibilities for particle detection and introduced a sensor design that shows a high sensitivity at a good spatial resolution. Due to the size of the sensors discussed here, they almost show no hysteresis as well. Therefore, a measured signal can readily be converted to a particle trajectory employing the calculated $\langle\alpha\rangle$ – surface.

For information on magnetic detection in micromagnetic simulations with COMSOL refer to the paper *Detection of Magnetic Particles by Magnetoresistive Sensors* in the current conference proceedings.

Literature

[1]C. Albon, A. Weddemann, A. Auge, K. Rott, A. Hütten, Appl. Phys. Lett. **95**, 023101 (2009)
[2]J. Loureiro et al., Appl. Phys. Lett. **95**, 034104 (2009)
[3]W. Schepper, J. Schotter, H. Brückl, G. Reiss, J. Biotechnol, **112**, 35 (2004)